Locally Range-Separated Hybrids as Linear Combinations of Range-Separated Local Hybrids

THOMAS M. HENDERSON,[1] **BENJAMIN G. JANESKO,**[1] **GUSTAVO E. SCUSERIA,**[1] **ANDREAS SAVIN**[2]

[1]*Department of Chemistry, Rice University, 6100 Main Street, Houston, TX 77005-1892*
[2]*Laboratoire de Chimie Théorique, CNRS, Université Pierre et Marie Curie, 4 Place Jussieu, F-75252 Paris, France*

Received 13 November 2008; accepted 9 December 2008
Published online 2 April 2009 in Wiley InterScience (www.interscience.wiley.com).
DOI 10.1002/qua.22049

ABSTRACT: Range-separated hybrid density functionals, which incorporate different fractions of exact exchange at different interelectronic separations, offer substantial advantages over conventional global hybrid functionals. However, they generally use a fixed, system-independent range-separation parameter, which numerical experience and formal arguments both show to be a limiting approximation. Locally range-separated hybrids, which instead use a position-dependent range-separation function, should overcome this limitation, but their implementation is nontrivial. Here, we present a method which in practice converts a locally range-separated hybrid into a linear combination of range-separated local hybrids. Thus, unlike our previous implementation of this locally range-separated hybrid idea, we do not need to approximate the exchange hole, and we can take advantage of existing self-consistent local hybrid implementations to carry out self-consistent calculations using locally range-separated hybrid functionals.
 Int J Quantum Chem 109: 2023–2032, 2009

Key words: local hybrids; local range separation; self-consistent

Correspondence to: G. E. Scuseria; e-mail: guscus@rice.edu
Contract grant sponsor: National Science Foundation.
Contract grant number: CHE-0807194.
Contract grant sponsor: Welch Foundation.
Contract grant number: C-0036.
Contract grant sponsor: French National Research Agency.
Contract grant number: ANR-07-BLAN-0272-03.
Contract grant sponsor: National Library of Medicine.
Contract grant number: 5T15LM07093.

1. Introduction

Because of its combination of low computational cost and reasonable accuracy, the Kohn–Sham [1, 2] (KS) construction in density functional theory (DFT) has over the past few decades become the dominant method in quantum chemistry [3]. The chief limitation in KS-DFT is the need to approximate the exchange-correlation functional $E_{xc}[n]$, which is known to be a functional of the electron density n, but whose precise dependence on the density is not known.

Simple semilocal functionals, such as the local density approximation (LDA), generalized gradient approximations (GGA), and meta-GGAs, write the exchange-correlation energy density at the point $\boldsymbol{r}$ as a function only of the density and possibly its derivatives and the kinetic energy density at that point. Although such functionals can be derived from first principles, their performance in practice is often inadequate for chemical purposes. To reach acceptable accuracy, it is common to use global hybrid functionals, which include a constant fraction of exact, nonlocal Hartree–Fock-type exchange [4–8]. At the cost of a single extra parameter (the fraction of exact exchange), global hybrids provide substantially better accuracy than their parent semilocal functionals. Global hybrids can be justified by adiabatic connection arguments, which allows the fraction of exact exchange to be chosen on theoretical, rather than empirical, grounds [4, 9, 10].

Although global hybrid functionals have done much to make KS-DFT the powerful tool it is today, they are not without their limitations. In extended systems, exact exchange is expensive to compute since the lattice sums required to evaluate it are slowly convergent. Moreover, as the band gap becomes small, long-range exact exchange is cancelled by long-range nondynamical correlation, and without explicit treatment of the latter, it is inappropriate to use the former [11]. On the other hand, exact exchange is required in finite systems, where it gives the correct asymptotic exchange-correlation potential, in contrast to that derived from semilocal functionals. As global hybrids include only a fraction of the nonlocal exchange interaction, they are in error for properties which sample density tails.

Many deficiencies of global hybrids can be corrected by using range-separated hybrids (RSH) [12, 13], in which the interelectronic Coulomb potential is split into short-range (SR) and long-range (LR) components, typically as

$$\frac{1}{r_{12}} = \underbrace{\frac{\mathrm{erf}(\omega r_{12})}{r_{12}}}_{\mathrm{LR}} + \underbrace{\frac{\mathrm{erfc}(\omega r_{12})}{r_{12}}}_{\mathrm{SR}}. \tag{1}$$

Once the Coulomb potential has been so separated, different fractions of exact exchange are used in different ranges.

By eliminating long-range exact exchange, screened hybrids such as the functional of Heyd, Scuseria, and Ernzerhof [14–16] improve both accuracy and affordability over global hybrids for extended systems. The HSE screened hybrid has accurately described, among other quantities, band gaps and lattice constants in semiconductors [17], in addition to performing well for molecular thermochemistry [18]. On the other hand, Hirao and others have shown that long-range-corrected hybrids incorporating 100% long-range exact exchange provide dramatic improvements for a host of properties sensitive to the decay of the density in finite systems [19–27]. More recently, some of us have emphasized the importance of middle-range exact exchange [18, 28].

Range-separated hybrids are not, however, a panacea. Several difficulties can be identified. Most importantly, range-separated hybrids in our formalisim require a model for the exchange hole corresponding to the desired semilocal exchange functional, and such models are not always available. Prescriptions for constructing such models have, however, been provided. Whether by using the LDA-based approach of Hirao and coworkers [19] or by using more complicated and functional-specific models [29–32], it is nowadays possible to construct exchange holes for arbitrary semilocal functionals.

Although this problem has largely been overcome, several others have not. Depending on the property under investigation, the optimal range-separation parameter ω can vary significantly [33]. Furthermore, different systems require different values of ω even for the same property. For example, the ω which returns the correct band gap in the HSE screened hybrid functional varies roughly between $0.05a_0^{-1}$ and $0.15a_0^{-1}$ [34], where a_0 is the Bohr radius. The ω which gives the correct dissociation curves for homonuclear diatomic cations X_2^+ is also known to be system-dependent [35]. System-dependent range-separation parameters have also been considered elsewhere [36].

In addition to these practical concerns, there is a formal concern as well. Because exact Kohn–Sham

exchange (i.e., Hartree–Fock-type exchange evaluated with Kohn–Sham orbitals) scales properly under uniform coordinate scaling [37] $\boldsymbol{r} \to \lambda \boldsymbol{r}$, global hybrids clearly do likewise, so long as they are implemented in the optimized effective potential sense [38, 39]. This is not true for conventional range-separated hybrids. A range-separated hybrid will scale correctly only so long as ωr_{12} is scale-invariant. This in turn requires that $\omega \to \omega/\lambda$; since $n(\boldsymbol{r}) \to \lambda^{-3} n(\lambda \boldsymbol{r})$ in order to keep the same normalization of n, we see that ω must scale as $n^{1/3}$ [37]. A simpler way to say this is just that ω must have dimensions of an inverse length, and the relevant length scale of the system is set by the density (whose dimensions are inverse volume).

We can begin to address these deficiencies of range-separated hybrids, all of which can be traced to the choice of ω, by making ω itself a local functional of the density. Although this idea has been proposed for range-separated correlation techniques [40, 41], it has proven difficult to implement. Recently, Krukau and coworkers proposed a semilocal ansatz in which the exact exchange hole is replaced by a model which is exact in certain limits [42]. In this work, we discuss a more rigorous implementation of locally range separated hybrids than the one presented in Ref. [42], and give illustrative results for a particular choice of the range-separation function.

2. Formalism

The exchange-correlation energy for a locally range-separated (LRS) hybrid can be written as

$$\begin{aligned} E_{\mathrm{xc}}^{\mathrm{LRS}} = E_{\mathrm{xc}}^{\mathrm{DFA}} &+ c_{\mathrm{SR}} \int d\mathbf{x} \left[\epsilon_x^{\mathrm{SR-HF}}(\mathbf{x}, \omega(\mathbf{x})) - \epsilon_x^{\mathrm{SR-DFA}}(\mathbf{x}, \omega(\mathbf{x})) \right] \\ &+ c_{\mathrm{LR}} \int d\mathbf{x} \left[\epsilon_x^{\mathrm{LR-HF}}(\mathbf{x}, \omega(\mathbf{x})) - \epsilon_x^{\mathrm{LR-DFA}}(\mathbf{x}, \omega(\mathbf{x})) \right], \end{aligned} \tag{2}$$

in terms of coefficients c_{SR} and c_{LR} and the short-range and long-range exact exchange (HF) and semilocal density functional approximation (DFA) exchange energy densities ϵ. The coordinate $\mathbf{x}$ is a space-spin coordinate with spatial part $\boldsymbol{r}$ and spin part σ; integration with respect to $\mathbf{x}$ denotes integration over space and summation over spin. The spatial integration in the foregoing equation can be done numerically on the usual DFT integration grid.

The long-range semilocal exchange energy density can be obtained simply via

$$\epsilon_x^{\mathrm{LR-DFA}}(\mathbf{x}_1, \omega) = \frac{1}{2} \int d\mathbf{x}_2 \, \frac{\mathrm{erf}(\omega r_{12})}{r_{12}} \, n(\mathbf{x}_1) h_x^{\mathrm{DFA}}(\mathbf{x}_1, r_{12}), \tag{3}$$

where $h_x^{\mathrm{DFA}}(\mathbf{x}_1, r_{12})$ is a semilocal model for the (spherically averaged) exchange hole, and where the integration with respect to $\mathbf{x}_2$ can usually be done analytically. An analogous expression holds for the short-range semilocal exchange energy density.

The complications for locally range-separated hybrids are all due to the range-separated exact exchange energy density. In the conventional gauge [43], the long-range exact exchange energy density is given by

$$\begin{aligned} \epsilon_x^{\mathrm{LR-HF}}(\mathbf{x}_1, \omega) = -\frac{1}{2} \sum_{i,j}^{\mathrm{occ}} &\varphi_i(\mathbf{x}_1) \varphi_j(\mathbf{x}_1) \\ &\times \int d\mathbf{x}_2 \varphi_j(\mathbf{x}_2) \, \frac{\mathrm{erf}(\omega r_{12})}{r_{12}} \, \varphi_i(\mathbf{x}_2). \end{aligned} \tag{4}$$

Although the integration with respect to $\mathbf{x}_2$ can be done analytically, there are $\mathcal{O}(N_{\mathrm{e}}^2)$ such integrations to be done at each grid point, where N_{e} is the number of electrons, so that the computational cost of evaluating the total exchange-correlation energy of Eq. (2) would scale as $\mathcal{O}(N_{\mathrm{e}}^2 N_{\mathrm{grid}})$, where N_{grid} is the number of points in the numerical integration grid. The computational cost of such an approach is thus too high for practical purposes.

Local hybrids [44–50] (which use a position-dependent admixture of exact exchange) face similar complications. There, one can employ a resolution of unity approximation originally suggested by Della Sala and Görling [51] to write

$$\begin{aligned} \epsilon_x^{\mathrm{HF}}(\mathbf{x}_1) \approx \epsilon_{x,\mathrm{DSG}}^{\mathrm{HF}}(\mathbf{x}_1) = -\frac{1}{2} \sum_{i,j}^{\mathrm{occ}} \sum_q &\\ \times \int d\mathbf{x}_2 d\mathbf{x}_3 \varphi_i(\mathbf{x}_1) \varphi_j(\mathbf{x}_2) \varphi_q(\mathbf{x}_3) \, \frac{1}{r_{23}} \, &\varphi_q(\mathbf{x}_1) \varphi_i(\mathbf{x}_2) \varphi_j(\mathbf{x}_3) \end{aligned} \tag{5}$$

where q runs over all molecular orbitals. Integrating with respect to $\mathbf{x}_2$ and $\mathbf{x}_3$, we obtain

$$\epsilon_{x,\mathrm{DFG}}^{\mathrm{HF}}(\mathbf{x}_1) = -\frac{1}{2} \sum_{i,j}^{\mathrm{occ}} \sum_q \varphi_i(\mathbf{x}_1) \varphi_q(\mathbf{x}_1) \left\langle \varphi_j \varphi_q \left| \frac{1}{r_{12}} \right| \varphi_i \varphi_j \right\rangle \tag{6}$$

where $\langle\varphi_p\varphi_q|1/r_{12}|\varphi_r\varphi_s\rangle$ is the usual two-electron integral in Dirac notation. The sum over j then gives us

$$\epsilon_{x,\mathrm{DSG}}^{\mathrm{HF}}(\mathbf{x}_1) = -\frac{1}{2}\sum_{i}^{\mathrm{occ}}\sum_{q}\varphi_i(\mathbf{x}_1)K_{iq}\varphi_q(\mathbf{x}_1), \quad (7)$$

where K_{iq} is a matrix element of the exact exchange operator. Note that integrating $\epsilon_{x,DSG}^{HF}(\mathbf{x})$ gives

$$\int d\mathbf{x}\epsilon_{x,\mathrm{DSG}}^{\mathrm{HF}}(\mathbf{x}) = -\frac{1}{2}\sum_{i}^{\mathrm{occ}}\sum_{q}K_{iq}\delta_{iq} = -\frac{1}{2}\sum_{i}^{\mathrm{occ}}K_{ii}, \quad (8)$$

which is the Hartree–Fock exchange energy. Since $\epsilon_x^{\mathrm{HF}}(\mathbf{x})$ and $\epsilon_{x,\mathrm{DSG}}^{\mathrm{HF}}(\mathbf{x})$ integrate to the same exchange energy even though they generally have local differences, we refer to the energy density of Eq. (7) as the exact exchange energy density in the Della Sala-Görling gauge. In practice, this is done in the atomic orbital basis set, which requires the evaluation also of the inverse of the atomic orbital overlap matrix.

A similar trick can be used when the electron repulsion operator is replaced with a range-separated operator, such as $\mathrm{erf}(\omega r_{12})/r_{12}$, which would give us

$$\epsilon_{x,\mathrm{DSG}}^{\mathrm{LR-HF}}(\mathbf{x}_1,\omega) = -\frac{1}{2}\sum_{i}^{\mathrm{occ}}\sum_{q}\varphi_i(\mathbf{x}_1)K_{iq}^{\mathrm{LR}}(\omega)\varphi_q(\mathbf{x}_1), \quad (9)$$

where

$$K_{iq}^{\mathrm{LR}}(\omega) = \sum_{j}^{\mathrm{occ}}\int d\mathbf{x}_1 d\mathbf{x}_2\varphi_i(\mathbf{x}_1)\varphi_j(\mathbf{x}_2)\frac{\mathrm{erf}(\omega r_{12})}{r_{12}} \times \varphi_j(\mathbf{x}_1)\varphi_q(\mathbf{x}_2). \quad (10)$$

Integrating this long-range exchange energy density yields the correct long-range exact exchange energy, and we can thus use the exchange energy densities of Eqs. (4) and (9) interchangeably in defining the total exchange-correlation energy of Eq. (2). In the case where ω depends on $\mathbf{x}_1$, however, such an approach would not reduce the computational scaling at all, since, ω presumably being different at each grid point, we would have to construct a different matrix $\mathbf{K}^{LR}(\omega)$ at each grid point.

To avoid this problem, Krukau, Scuseria, Perdew, and Savin [42] proposed to construct a semilocal (and thus analytically integrable) model of the exact exchange hole, constrained so that it correctly reproduces the full range exact exchange energy density. Then the long-range exact exchange energy density would be written as

$$\epsilon_x^{\mathrm{LR-HF}}(\mathbf{x}_1,\omega) \approx \frac{1}{2}\int d\mathbf{x}_2\frac{\mathrm{erf}(\omega r_{12})}{r_{12}}n(\mathbf{x}_1) \times h_x\big(\mathbf{x}_1, r_{12}; \epsilon_x^{\mathrm{HF}}(\mathbf{x}_1)\big), \quad (11)$$

where the dependence of the semilocal model exchange hole h_x on the full range exact exchange energy density is included for emphasis. This model integrates to the correct long-range exact exchange energy as ω goes to zero or infinity, but not for other values of ω.

We here suggest a different approximation, in which for a variable ω depending on position we write

$$\mathrm{erf}(\omega(\mathbf{x})r_{12}) \approx \sum_{\mu}c_\mu(\omega(\mathbf{x}))\mathrm{erf}(\omega_\mu r_{12}). \quad (12)$$

Here, the ω_μ are fixed parameters providing a basis for expanding $\omega(\mathbf{x})$. By making this approximation, we are able to write

$$\epsilon_{x,\mathrm{DSG}}^{\mathrm{LR-HF}}(\mathbf{x},\omega(\mathbf{x})) \approx -\frac{1}{2}\sum_{i}^{\mathrm{occ}}\sum_{q}\sum_{\mu}c_\mu(\omega(\mathbf{x})) \times \varphi_i(\mathbf{x})K_{iq}^{\mathrm{LR}}(\omega_\mu)\varphi_q(\mathbf{x}) \quad (13a)$$

$$= \sum_{\mu}c_\mu(\omega(\mathbf{x}))\epsilon_{x,\mathrm{DSG}}^{\mathrm{LR-HF}}(\mathbf{x},\omega_\mu). \quad (13b)$$

To ensure that we treat the exact exchange component and the semilocal exchange component to equal accuracy, we also write

$$\epsilon_x^{\mathrm{LR-DFA}}(\mathbf{x},\omega(\mathbf{x})) \approx \sum_{\mu}c_\mu(\omega(\mathbf{x}))\epsilon_x^{\mathrm{LR-DFA}}(\mathbf{x},\omega_\mu), \quad (14)$$

so that the total exchange-correlation energy becomes

$$E_{\mathrm{xc}}^{\mathrm{LRS}} = E_{\mathrm{xc}}^{\mathrm{DFA}} + c_{\mathrm{SR}}\sum_{\mu}\int d\mathbf{x}c_\mu(\omega(\mathbf{x})) \times\left[\epsilon_{x,\mathrm{DSG}}^{\mathrm{SR-HF}}(\mathbf{x},\omega_\mu) - \epsilon_x^{\mathrm{SR-DFA}}(\mathbf{x},\omega_\mu)\right] + c_{\mathrm{LR}}\sum_{\mu}\int d\mathbf{x}c_\mu(\omega(\mathbf{x})) \times\left[\epsilon_{x,\mathrm{DSG}}^{\mathrm{LR-HF}}(\mathbf{x},\omega_\mu) - \epsilon_x^{\mathrm{LR-DFA}}(\mathbf{x},\omega_\mu)\right]. \quad (15)$$

Effectively, we have transformed a locally range-separated hybrid into a linear combination of local

hybrids. As the number of fixed parameters ω_μ gets large, the range-separated exchange energy density we have proposed becomes identical to the long-range exact exchange energy density in the Della Sala-Görling gauge. This model can thus be used without introducing any errors in the range-separated exact exchange energy, so long as we are willing to pay the price of letting the number of expansion parameters become large enough. An additional benefit is that, as the exchange energy density of Eq. (13) takes the local hybrid form, self-consistent implementation in the generalized Kohn–Sham approach is straightforward with our recently developed codes [52].

Before turning our attention to the details of our algorithm, let us briefly discuss the choice of $\omega(\mathbf{x})$. Assuming that $\omega(\mathbf{x})$ depends only on the spin-density $n(\mathbf{x})$ and on $\nabla n(\mathbf{x})$, the scaling consideration previously discussed suggests

$$\omega(\mathbf{x}) = k_F(\mathbf{x})F(s(\mathbf{x})), \tag{16a}$$

$$k_F(\mathbf{x}) = (6\pi^2 n(\mathbf{x}))^{1/3}, \tag{16b}$$

$$s(\mathbf{x}) = \frac{|\nabla n(\mathbf{x})|}{2k_F(\mathbf{x})n(\mathbf{x})}. \tag{16c}$$

The work of Krukau et al. [42] suggests that $F(s) = \zeta s$ is a reasonable starting point. Our focus here is on the algorithmic details of our proposed approach and not on the optimal choice of $\omega(\mathbf{x})$, but we will briefly discuss the numerical performance of this choice of $\omega(\mathbf{x})$ as a function of ζ.

3. Algorithmic Details

To construct the exchange energy density of Eq. (13), we need to address two main issues. First, we must give a prescription for $c_\mu(\omega)$, and second, we must choose the ω_μ. Although the former is straightforward, the latter requires no little thought.

To construct $c_\mu(\omega)$, we simply use a Lagrange interpolation form. That is, we write

$$c_\mu(\omega) = \prod_{\nu\neq\mu} \frac{\omega - \omega_\nu}{\omega_\mu - \omega_\nu}. \tag{17}$$

Because

$$\sum_\mu c_\mu(\omega) = 1, \tag{18a}$$

$$\sum_\mu c_\mu(\omega)\omega_\mu = \omega, \tag{18b}$$

our approximation for the error function is exact at small r_{12} (where the error function is linear in ωr_{12}) and at large r_{12} (where the error function approaches one). Further, Eq. (18a) implies that we can use the same expansion coefficients $c_\mu(\omega)$ for $\mathrm{erf}(\omega r_{12})$ and for $\mathrm{erfc}(\omega r_{12})$:

$$\mathrm{erfc}(\omega r_{12}) = 1 - \mathrm{erf}(\omega r_{12}) \tag{19a}$$

$$\approx \sum_\mu c_\mu(\omega) - \sum_\mu c_\mu(\omega)\mathrm{erf}(\omega_\mu r_{12}) \tag{19b}$$

$$\approx \sum_\mu c_\mu(\omega)\mathrm{erfc}(\omega_\mu r_{12}). \tag{19c}$$

To choose the ω_μ, we pick smallest and largest values, respectively $\omega_{\min}$ and $\omega_{\max}$, along with the number N_ω of expansion functions. Given $\omega_{\min}$, $\omega_{\max}$, and N_ω, there are two simple schemes for picking the ω_μ. One could use an equally spaced grid,

$$\omega_\mu = \frac{\omega_{\min} + \omega_{\max}}{2} + \frac{\omega_{\max} - \omega_{\min}}{2}\frac{2\mu - N_\omega - 1}{N_\omega - 1}, \tag{20}$$

or a Chebyshev grid,

$$\omega_\mu = \frac{\omega_{\min} + \omega_{\max}}{2} + \frac{\omega_{\max} - \omega_{\min}}{2}\cos\left(\frac{2\mu - 1}{2N_\omega}\pi\right). \tag{21}$$

Uniform grids are susceptible to Runge's phenomenon, in which the interpolating polynomial oscillates around the exact curve, with the oscillations growing larger in magnitude as the order of the interpolating polynomial (i.e., N_ω) grows. This problem is mitigated by using a Chebyshev grid, which we therefore prefer.

It yet remains to choose N_ω, $\omega_{\min}$, and $\omega_{\max}$. We discuss these below.

3.1. Sensitivity to the Number of Expansion Functions

To investigate the sensitivity to the number of expansion functions, we show in Figure 1 the error function and the expansion of Eq. (12) for two choices of $\omega_{\min}$, $\omega_{\max}$, and for several choices of N_ω.

As the figure illustrates, we clearly need more than two expansion functions, and would prefer to use more than four; six seems to be sufficient. This can be verified by considering long-range-corrected LDA [53, 54], which uses 100% short range LDA exchange and 100% long range exact exchange. Here and in the rest of this work, we refer to this functional as LC-ωLDA and set $\omega = 0.60a_0^{-1}$. Treating LC-ωLDA as a

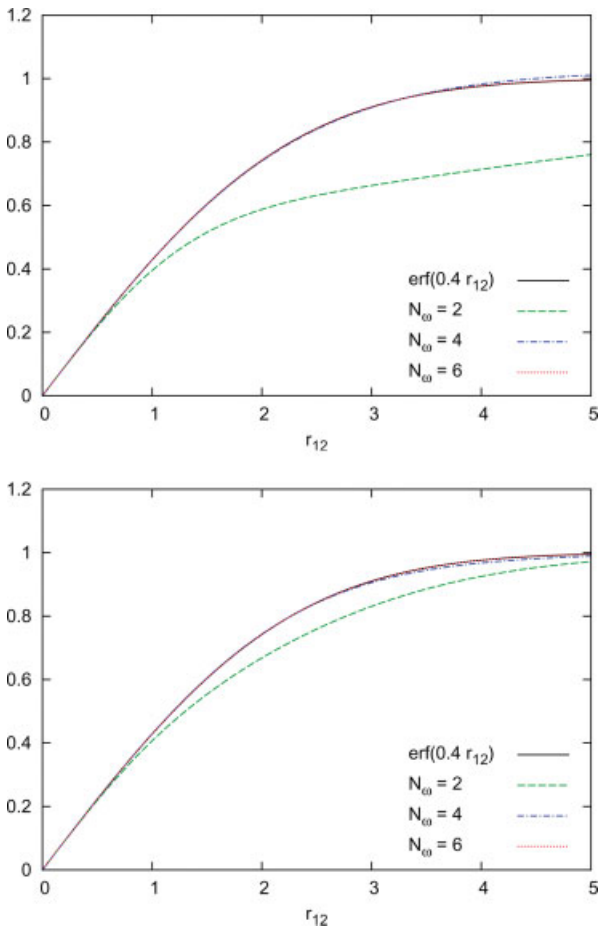

FIGURE 1. Error function and its interpolation. Both panels use an evenly spaced grid of ω_μ, and interpolate $\mathrm{erf}(0.4r_{12})$. Top panel: $\omega_{\mathrm{min}} = 0.1$ and $\omega_{\mathrm{max}} = 0.7$. Bottom panel: $\omega_{\mathrm{min}} = 0.3$ and $\omega_{\mathrm{max}} = 0.9$. In both cases, the lines for $N_\omega = 4$, $N_\omega = 6$, and the exact error function are essentially superimposable. [Color figure can be viewed in the online issue, which is available at www.interscience.wiley.com.]

locally range-separated hybrid with $\omega(\mathbf{x}) = 0.60a_0^{-1}$, we can compare the results using our approach [Eq. (15)] to the exact results for the functional. Accordingly, we calculate the mean absolute error (MAE) in the AE6 and BH6 sets of atomization energies and barrier heights [55], as well as in the total energies of the first eighteen atoms (H-Ar) [56]. Results are displayed in Table I. We see that with six expansion functions, the interpolation error is negligible. Note, however, that as $\omega_{\mathrm{max}} - \omega_{\mathrm{min}}$ becomes larger compared to $(\omega_{\mathrm{max}} + \omega_{\mathrm{min}})/2$, the number of expansion functions required for accurate interpolation increases.

To show that the interpolation of Eq. (12) is uniformly accurate between ω_{min} and ω_{max}, we examine

TABLE I

Comparison between results from the long-range-corrected LC-ωLDA functional evaluated exactly and approximately, via the interpolation of Eq. (12).

N_ω	AE6	BH6	Atoms
2	13.117	2.009	43.081
4	11.020	2.477	42.817
6	11.127	2.495	42.812
LC-ωLDA	11.131	2.493	42.812

Although LC$-\omega$LDA uses $\omega = 0.60a_0^{-1}$, the interpolation uses $\omega_{\mathrm{min}} = 0.30a_0^{-1}$, $\omega_{\mathrm{max}} = 0.90a_0^{-1}$, and a number of expansion functions varying from 2 to 6. We do not consider odd values for N_ω, since in that case the interpolation is exact as one of the expansion functions uses $\omega = 0.60a_0^{-1}$. We show mean absolute errors (MAE) in kcal/mol for the AE6 and BH6 sets, and in mH/electron for the total energies of H-Ar.

the long-range-corrected LDA functional as a function of ω. In Figure 2, we show the MAE for the AE6 set (kcal/mol), the BH6 set (kcal/mol), and H-Ar (mH/electron) from LC-ωLDA. We also show the results from the interpolation of Eq. (12) with $\omega_{\mathrm{min}} = 0.20a_0^{-1}$, $\omega_{\mathrm{max}} = 1.00a_0^{-1}$, and $N_\omega = 6$. Clearly, the interpolation is accurate across the whole range of ω. Note that these results use LC-ωLDA orbitals with $\omega = 0.60a_0^{-1}$.

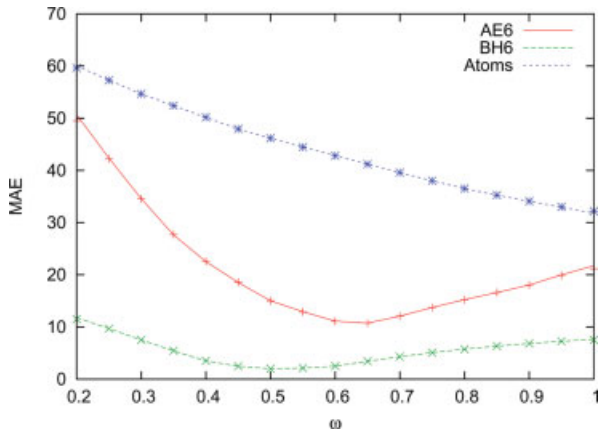

FIGURE 2. Mean absolute error for LC-ωLDA as a function of ω, and for the same functional using the linear combination of error functions as in Eq. (12). We set $N_\omega = 6$, $\omega_{\mathrm{min}} = 0.20a_0^{-1}$, and $\omega_{\mathrm{max}} = 1.00a_0^{-1}$. Results evaluating the error function exactly are shown as lines; results using the linear combination of error functions are shown as points. [Color figure can be viewed in the online issue, which is available at www.interscience.wiley.com.]

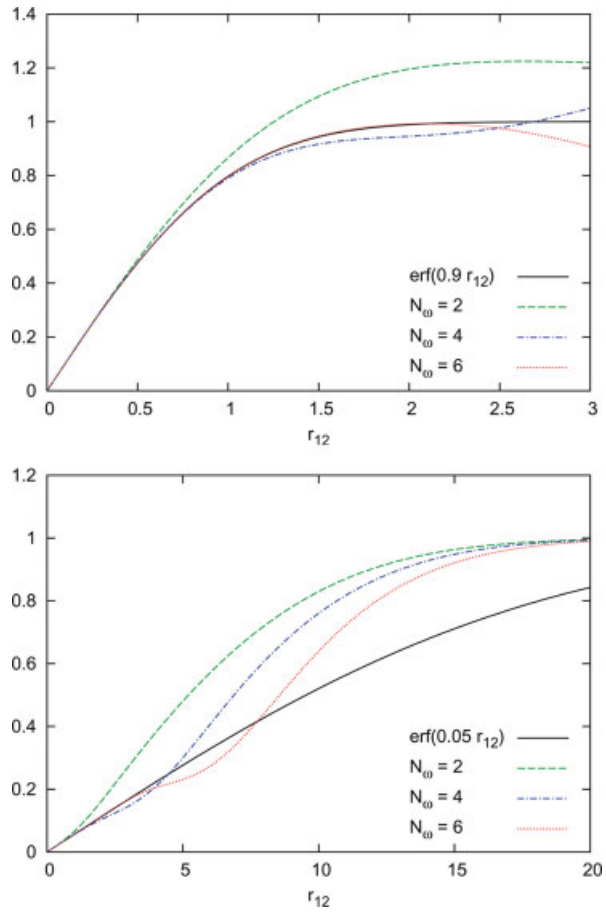

FIGURE 3. Error function and its extrapolation. Both panels use an evenly spaced grid of ω_μ, with $\omega_{\min} = 0.1$ and $\omega_{\max} = 0.7$. Top panel: $\omega = 0.9$. Bottom panel: $\omega = 0.05$. [Color figure can be viewed in the online issue, which is available at www.interscience.wiley.com.]

3.2. CHOOSING $\omega_{\min}$ AND $\omega_{\max}$

The previous section establishes that for $\omega_{\min} < \omega < \omega_{\max}$, we can reliably expand $\mathrm{erf}(\omega r)$. But while accurate interpolation is straightforward, accurate extrapolation is problematic at best. This is illustrated by Figure 3, which shows the expansion of Eq. (12) when $\omega > \omega_{\max}$ or $\omega < \omega_{\min}$.

As our expansion is clearly inadequate for extrapolation, we wish to force ω to lie between $\omega_{\min}$ and $\omega_{\max}$ at every point in space. In other words, if we find $\omega > \omega_{\max}$ we wish to replace ω with $\omega_{\max}$, and similarly for $\omega < \omega_{\min}$. Since we need $\omega(\mathbf{x})$ to be differentiable, we must find a smooth function that does this.

A one-parameter function that suffices is

$$F(x,a,Z) = -\frac{1}{a}\log\left(\frac{e^{-ax} + b(aZ)}{1 + b(aZ)}\right), \qquad (22)$$

where

$$b(aZ) = \frac{1}{e^{aZ} - 1}. \qquad (23)$$

When ax is small, $F(x,a,Z) \sim x/(1+b)$, and when ax is large, $F(x,a,Z) \sim Z$. We also know that $1/F(1/x,a,1/Z)$ approaches Z when a/x is large, and $(1+b)x$ when a/x is small. We can thus rescale ω as

$$\omega \longrightarrow \bar{\omega} = F\left(\frac{1}{F(1/\omega, a_1, 1/\omega_{\min})}, a_2, \omega_{\max}\right). \qquad (24)$$

We want a_1 and a_2 to be such that $b(a_2\omega_{\max})$ and $b(a_1/\omega_{\min})$ are small, so that we have minimal difference between ω and $\bar{\omega}$; we thus write $a_1 = 20\omega_{\min}$ and $a_2 = 40/\omega_{\max}$. By rescaling ω in this way, we remove any extrapolation error. However, we do not eliminate the dependence of our result on the choices of $\omega_{\min}$ and $\omega_{\max}$.

Because the range-separated exchange-correlation energy depends on the difference between exact exchange and semilocal exchange energy densities [*c.f.* Eq. (15)], we do not need to accurately evaluate $\epsilon_x^{\mathrm{LR-HF}}(\mathbf{x}, \omega(\mathbf{x}))$, but rather $\epsilon_x^{\mathrm{LR-HF}}(\mathbf{x}, \omega(\mathbf{x})) - \epsilon_x^{\mathrm{LR-DFA}}(\mathbf{x}, \omega(\mathbf{x}))$. We assume chemistry is not strongly affected by changing ω in the atomic core. Our goal, then, is to choose $\omega_{\min}$ and $\omega_{\max}$ such that we can evaluate the difference of range-separated exchange energy densities in the valence region with good accuracy.

As an example, we consider the Ar atom and the CO molecule with $\omega = \zeta k_F s$. In Figure 4, we show ω in the Ar atom as a function of the distance from the nucleus, and in the CO molecule along the bond axis. We also show the rescaled variable $\bar{\omega}$, where we have made the choice $\omega_{\min} = \zeta/2$ and $\omega_{\max} = 6\zeta$. With this choice, the rescaling affects only the Ar and O cores, and the low-gradient regions of the CO bond (where semilocal functionals and exact exchange are similar); elsewhere, ω and $\bar{\omega}$ are indistinguishable.

4. Results

To validate our approach, we evaluate the locally range-separated hybrid with $\omega = \zeta k_F s$, in accordance with Ref. [42]. We consider the AE6 set of six atomization energies [55], the BH6 set of six reaction barriers [55], and the total atomic energies of H-Ar [56]. We show results for a locally range-separated version of LC-ωLDA, using the uncontracted 6-311++G(3df,3pd) basis set. As before, we take

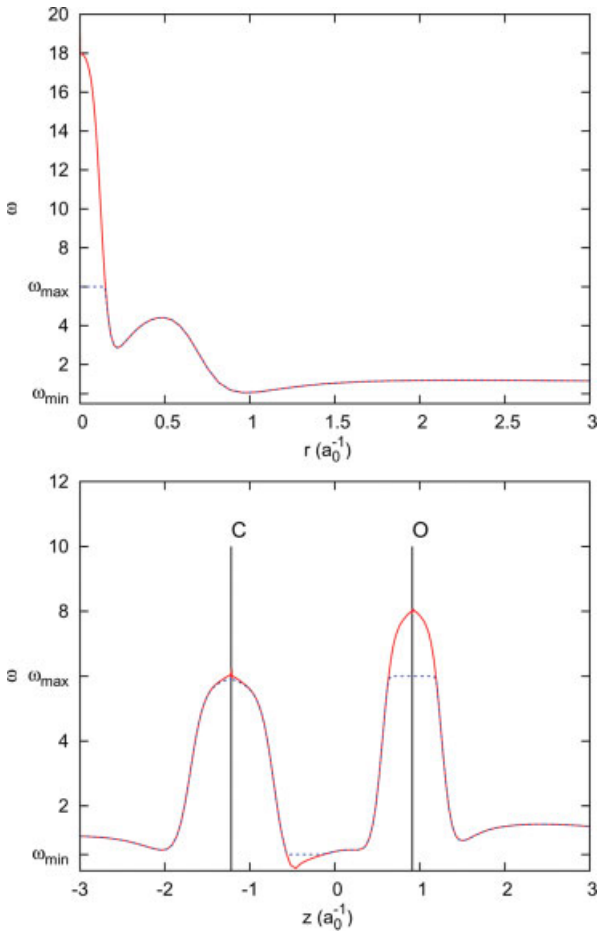

FIGURE 4. Range-separation function $\omega = \zeta k_F s$ in units of ζ as a function of the distance from the nucleus in the Ar atom (top panel) and along the bond axis of CO (bottom panel). Also shown is the rescaled variable $\bar{\omega}$ (dashed lines), which is superimposable with ω almost everywhere. [Color figure can be viewed in the online issue, which is available at www.interscience.wiley.com.]

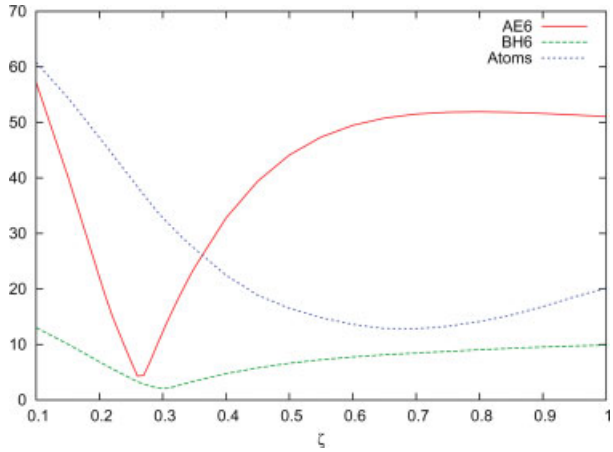

FIGURE 5. Mean absolute error for the locally range-separated long-range-corrected hybrid of LSDA with $\omega = \zeta k_F s$ as a function of ζ for the AE6 and BH6 sets (kcal/mol) and total atomic energies of H-Ar (mH/electron). [Color figure can be viewed in the online issue, which is available at www.interscience.wiley.com.]

$N_\omega = 6$ and choose $\omega_{\min} = \zeta/2$ and $\omega_{\max} = 6\zeta$. In this initial validation, we show non-self-consistent results using LC-ωLDA orbitals.

In Figure 5 we show mean absolute errors (MAE) as a function of ζ. Results are given in kcal/mol for the AE6 and BH6 sets, and in mH/electron for total atomic energies. While atomic total energies are poorly described, as is typical of hybrids of LSDA, we see that for $\zeta \sim 0.25 - 0.3$ both atomization energies and barrier heights are fairly well described. The very sharp minimum in the errors for atomization energies can be traced to the mean signed error changing signs between $\zeta = 0.26$ and $\zeta = 0.27$. Interestingly, the results for atomization energies are in good agreement with those of Krukau et al., despite the differences between our treatment of the locally range-separated exact exchange energy and those of Ref. [42]. Results for atomic total energies disagree significantly (by about 10 mH/electron). This may be due in part to differences in the treatment of core electrons.

We close by considering the effects of changing a few key parameters in the calculations, focusing on the case $\zeta = 0.27$. In Table II, we show results for the self-consistent (SC) and nonself-consistent (NSC)

TABLE II

Effects of increasing N_ω or iterating to self-consistency on the mean absolute errors in the AE6 and BH6 sets (kcal/mol) and the total atomic energies of H-Ar (mH/electron) for the locally range-separated LC-ωLDA with $\omega = 0.27 k_F s$.

Calculation	AE6	BH6	Atoms
$N_\omega = 6$, NSC	4.4	2.9	37.0
$N_\omega = 6$, SC	4.0	3.2	36.8
$N_\omega = 8$, NSC	4.5	2.8	37.0
$N_\omega = 8$, SC	4.2	3.3	36.8
Local Hybrid	3.5	3.0	30.5

"SC" and "NSC" denote self-consistent and nonself-consistent, respectively. We have also included self-consistent results for the local hybrid with mixing function $c = 0.48\ \tau_W/\tau$ for comparison.

calculations with $N_\omega = 6$ and $N_\omega = 8$. Clearly, neither self-consistency nor increasing N_ω has a large effect, though combining both exarcebates the differences somewhat. We should point out that the sensitivity to N_ω increases somewhat as we increase ζ, at least for non-self-consistent calculations; with this choice of ω_{min} and ω_{max}, $N_\omega = 8$ may be preferred.

For the case $N_\omega = 8$, non-self-consistent calculations adjusting ω_{min} by $\pm 10\%$ changes the atomization energies by $\sim$0.1 kcal/mol and has a negligible effect on the barrier heights and atomic total energies. Results with ω_{max} changing by $\pm 5\%$ show similar behavior – atomization energies change by $\sim$0.2 kcal/mol, barrier heights are unaffected, and atomic total energies change by $\sim$0.5 mH/electron (presumably due to differences in the description of the core). Interestingly, as ω_{max} is varied further, and especially as it is further decreased, atomization energies are more strongly affected. The cause of this behavior is not entirely clear.

5. Conclusions

Range-seprated hybrids have begun to come into their own as important tools in quantum chemistry. We anticipate that, in time, locally range-separated hybrids will do likewise. For this to happen, however, techniques for the accurate and effcient evaluation of the locally range-separated exchange-correlation energy are required. We have presented one such technique.

By making use of the expansion of Eq. (12), we can cast the locally range-separated hybrid in a computationally tractable form, without needing to approximate the exact exchange hole. Furthermore, self-consistent implementation starting from a self-consistent implementation of local hybrids in the generalized Kohn–Sham [40] scheme is straightforward. Within the range $\omega_{\text{min}} \leq \omega \leq \omega_{\text{max}}$, the approach given here is accurate and systematic – as N_ω becomes large, we recover the same result we would have obtained had we constructed the exact exchange energy density of Eq. (9) exactly.

The computational cost of our approach is rather higher than that of the approach taken by Krukau et al., since at each SCF iteration we must form N_ω versions of the exact exchange energy density, rather than one. Because the scheme presented here is ill-suited to describing very large or very small values of ω, and that given in Ref. [42] is best suited to these ranges, the two techniques are complementary. We speculate that an ideal approximation would be to use the scheme presented there to handle the cases $\omega > \omega_{\text{max}}$ and $\omega < \omega_{\text{min}}$, while using the approach presented here to handle $\omega_{\text{min}} \leq \omega \leq \omega_{\text{max}}$.

References

1. Dreizler, R. M.; Gross, E. K. U. Density Functional Theory; Plenum Press: New York, 1995.
2. Parr, R. G.; Yang, W. Density Functional Theory of Atoms and Molecules; Oxford University Press: New York, 1989.
3. Scuseria, G. E.; Staroverov, V. N. Progress in the development of exchange-correlation functionals. In Theory and Applications of Computational Chemistry: The First 40 Years; Dykstra, C. E.; Frenking, G.; Kim, K. S.; Scuseria, G. E., Eds.; Elsevier: Amsterdam, 2005.
4. Becke, A. D. J Chem Phys 1993, 98, 1372.
5. Becke, A. D. J Chem Phys 1993, 98, 5648.
6. Stephens, P. J.; Devlin, F. J.; Chabalowski, C. F.; Frisch, M. J. J Phys Chem 1994, 98, 11623.
7. Ernzerhof, M.; Scuseria, G. E. J Chem Phys 1999, 110, 5029.
8. Adamo, C.; Barone, V. J Chem Phys 1999, 110, 6158.
9. Becke, A. D. J Chem Phys 1993, 98, 5648.
10. Perdew, J. P.; Ernzerhof, M.; Burke, K. J Chem Phys 1996, 105, 9982.
11. Monkhorst, H. J. Phys Rev B 1979, 20, 1504.
12. Savin, A. In Recent Developments and Applications of Modern Density Functional Theory; Seminario, J. M., Ed.; Elsevier: Amsterdam, 1996.
13. Leininger, T.; Stoll, H.; Werner, H.-J.; Savin, A. Chem Phys Lett 1997, 275, 151.
14. (a) Heyd, J.; Scuseria, G. E.; Ernzerhof, M. J Chem Phys 2003, 118, 8207; (b) Heyd, J.; Scuseria, G. E.; Ernzerhof, M. J Chem Phys 2006, (E)124, 219906.
15. Heyd, J.; Scuseria, G. E. J Chem Phys 2004, 120, 7274.
16. Heyd, J.; Scuseria, G. E. J Chem Phys 2004, 121, 1187.
17. Heyd, J.; Peralta, J. E.; Scuseria, G. E.; Martin, R. L. J Chem Phys 2005, 123, 174101.
18. Henderson, T. M.; Izmaylov, A. F.; Scuseria, G. E.; Savin, A. J Comp Theor Chem 2008, 4, 1254.
19. Iikura, H.; Tsuneda, T.; Yanai, T.; Hirao, K. J Chem Phys 2001, 115, 3540.
20. Tawada, Y.; Tsuneda, T.; Yanagisawa, S.; Yanai, T.; Hirao, K. J Chem Phys 2004, 120, 8425.
21. Sekino, H.; Maeda, Y.; Kamiya, M. Mol Phys 2005, 103, 2183.
22. Kamiya, M.; Sekino, H.; Tsuneda, T.; Hirao, K. J Chem Phys 2005, 122, 234111.
23. Kamiya, M.; Tsuneda, T.; Hirao, K. J Chem Phys 2002, 117, 6010.
24. Sato, T.; Tsuneda, T.; Hirao, K. J Chem Phys 2005, 123, 104307.
25. Ángyán, J. G.; Gerber, I. C.; Savin, A.; Toulouse, J. Phys Rev A 2005, 72, 012510.
26. Goll, E.; Werner, H.-J.; Stoll, H. Phys Chem Chem Phys 2005, 7, 3917.
27. Vydrov, O. A.; Scuseria, G. E. J Chem Phys 2006, 125, 234109.

28. Henderson, T. M.; Izmaylov, A. F.; Scuseria, G. E.; Savin, A. J Chem Phys 2007, 127, 221103.
29. Ernzerhof, M.; Perdew, J. P. J Chem Phys 1998, 109, 3313.
30. Constantin, L. A.; Perdew, J. P.; Tao, J. Phys Rev B 2006, 73, 205104.
31. Henderson, T. M.; Janesko, B. G.; Scuseria, G. E. J Chem Phys 2008, 128, 194105.
32. Bahmann, H.; Ernzerhof, M. J Chem Phys 2008, 128, 234104.
33. Song, J.-W.; Hirosawa, T.; Tsuneda, T.; Hirao, K. J Chem Phys 2007, 126, 154105.
34. Brothers, E. N.; Izmaylov, A. F.; Normand, J. O.; Barone, V.; Scuseria, G. J Chem Phys 2008, 129, 011102.
35. Livshits, E.; Baer, R. A density functional theory for symmetric radical cations from bonding to dissociation. Available at: http://www.citebase.org/abstract?id=oai:arXiv.org:0804.3415. 2008.
36. Bylander, D. M.; Kleinman, L. Phys Rev B 1990, 41, 7868.
37. Levy, M.; Perdew, J. P. Phys Rev A 1985, 32, 2010.
38. Sharp, R. T.; Horton, G. K. Phys Rev 1953, 90, 317.
39. Talman, J. D.; Shadwick, W. F. Phys Rev A 1976, 14, 36.
40. Seidl, A.; Görling, A.; Vogl, P.; Majewski, J. A.; Levy, M. Phys Rev B 1996, 53, 3764.
41. Toulouse, J.; Colonna, F.; Savin, A. J Chem Phys 2005, 122, 014110.
42. Krukau, A. V.; Scuseria, G. E.; Perdew, J. P.; Savin, A. J. Chem Phys 2008, 129, 124103.
43. Tao, J.; Staroverov, V. N.; Scuseria, G. E.; Perdew, J. P. Phys Rev A 2008, 77, 012509.
44. Burke, K.; Cruz, F. G.; Lam, K.-C. J Chem Phys 1998, 109, 8161.
45. Jaramillo, J.; Scuseria, G. E.; Ernzerhof, M. J Chem Phys 2003, 118, 1068.
46. Janesko, B. G.; Scuseria, G. E. J Chem Phys 2007, 127, 164117.
47. Bahmann, H.; Rodenberg, A.; Arbuznikov, A. V.; Kaupp, M. J Chem Phys 2007, 126, 011103.
48. Arbuznikov, A. V.; Kaupp, M. Chem Phys Lett 2007, 440, 160.
49. Kaupp, M.; Bahmann, H.; Arbuznikov, A. V. J Chem Phys 2007, 127, 194102.
50. Janesko, B. G.; Scuseria, G. E. J Chem Phys 2008, 128, 084111.
51. Sala, F. D.; Görling, A. J Chem Phys 2001, 115, 5718.
52. Janesko, B. G.; Krukau, A. V.; Scuseria, G. E. J Chem Phys 2008, 129, 124110.
53. Gerber, I. C.; Ángyán, J. G. Chem Phys Lett 2005, 415, 100.
54. Vydrov, O. A.; Heyd, J.; Krukau, A. V.; Scuseria, G. E. J Chem Phys 2006, 125, 074106.
55. (a) Lynch, B. J.; Truhlar, D. G. J Phys Chem A 2003, 107, 8996; (b) Lynch, B. J.; Truhlar, D. G. J Phys Chem A 2004, E108, 1460.
56. Chakravorty, S. J.; Gwaltney, S. R.; Davidson, E. R.; Parpia, F. A.; Fischer, C. F. Phys Rev A 1993, 47, 3649.